Desalination and Water Treatment
www.deswater.com

doi: 10.5004/dwt.2017.21109

81 (2017) 282–290
June

Preparation of TiO_2-based photocatalysts and their photocatalytic degradation properties for methylene blue, rhodamine B and methyl orange

Jin-Gang Yu[a,*], Jiao Zou[a], Liang-Liang Liu[b], Xin-Yu Jiang[a], Fei-Peng Jiao[a], Xiao-Qing Chen[a]

[a]*College of Chemistry and Chemical Engineering, Hunan Provincial Key Laboratory of Efficient and Clean Utilization of Manganese Resources, Central South University, Changsha, Hunan 410083, China, Tel./Fax: +86-731-88879616; email: yujg@csu.edu.cn (J.-G. Yu)*
[b]*Institute of Bast Fiber Crops, Chinese Academy of Agricultural Sciences, Changsha 410205, China*

Received 4 April 2017; Accepted 2 July 2017

ABSTRACT

Different kinds of nanocrystalline TiO_2-based photocatalysts, including pristine TiO_2, oxidized multi-walled carbon nanotube/TiO_2 (ox-MWCNT/TiO_2) composite and Eu^{3+}-doped ox-MWCNT/TiO_2 (Eu^{3+}/ox-MWCNT/TiO_2) composite, were synthesized by using tetrabutyl titanate as precursor by a sol–gel method. The colloidal solutions were heat treated at 450°C for 2 h to obtain the anatase TiO_2 nanomaterials. The photocatalysts were characterized by X-ray diffraction, high-resolution transmission electron microscopy and energy-dispersive X-ray spectroscopy. The photocatalytic activities of the TiO_2-based catalysts for the degradation of methylene blue (MB), rhodamine B (RhB) and methyl orange (MO) in aqueous solutions were investigated. To compare the photocatalytic activity of the TiO_2-based catalysts, the degradation rates for the abovementioned dyes under 365 nm ultraviolet (UV) light irradiation were calculated. And the 1% Eu^{3+}/ox-MWCNT/TiO_2 composite showed higher photodegradation rate constant (K' = 1.757 h^{-1}) than those of pristine TiO_2 (K' = 1.028 h^{-1}), ox-MWCNT/TiO_2 (K' = 1.458 h^{-1}) and 4% Eu^{3+}/ox-MWCNT/TiO_2 composite (K' = 1.295 h^{-1}) toward MB. Meanwhile, the 1% Eu^{3+}/ox-MWCNT/TiO_2 composite possessed high photodegradation percentage of 95.77%, 97.21% and 90.72% toward RhB, MB and MO, respectively, which were higher than those of other three TiO_2-based photocatalysts. It is proposed that the higher photocatalytic activity of ox-MWCNT/Eu^{3+}/TiO_2 composite might be due to the decreased band gap, the plentiful introduced hydroxyl groups and its high specific surface area.

Keywords: Methylene blue; Rhodamine B; Methyl orange; Photocatalytic degradation; TiO_2

1. Introduction

Because of the water crisis, the necessity of protecting the ecological environment water supply has drawn much attention in recent years [1]. Some of the most common poisonous organic dyes such as methylene blue (MB), rhodamine B (RhB) and methyl orange (MO) (Fig. 1) are discharging from plastics, textiles and paint industries, which are considered as the primary pollutants in natural waters [2]. And in general, the application of various adsorbents for removal of the dyes from water is considered as one of the most important approaches [3–5].

To remove the harmful dyes from a water supply and make it fit for human consumption and regular use, there is no doubt that water remediation has to be performed. However, great challenges are often posed by the low adsorption capacities and poor cycling capabilities of the adsorbents. The degradation of dyes in contaminated water has therefore received increasing attention due to its high efficiency and low cost [6,7]. Up to now, various photocatalysts have been developed [8–15]. Among the existing catalysts, TiO_2-based materials have attracted much attention due to the high efficiencies activated by UV irradiation ($\lambda \leq 387$ nm) [16–19]. To promote its degradation efficiency for organic contaminants, doping process coupled with surface nanocrystallization were found to be beneficial due to the improvement in

* Corresponding author.

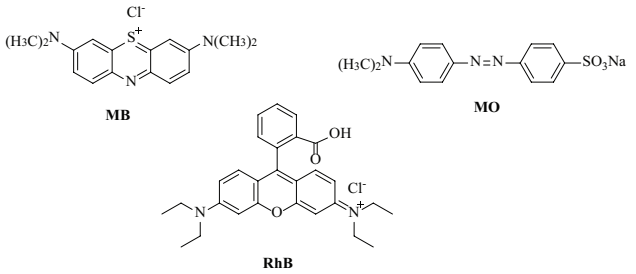

Fig. 1. Chemical structures of MB, MO and RhB.

the active surface area and the introduced excellent electric properties. The researchers have developed different novel methods of doping various metals, nonmetals or nanostructures such as boron (B) [20], trivalent europium (Eu^{3+}) [21], quadrivalent silicon (Si^{4+}) [22], carbon nanotubes (CNTs) [23], clinoptilolite nanoparticles [24,25], transition metal ions [26] and so on into the TiO_2 lattice, and the photocatalytic activities of the doped compounds could be greatly enhanced.

Due to their remarkable electrical and mechanical properties, carbon-based nanomaterials such as CNTs, graphene and graphene oxide have received significant attention in the field of material science [27–30], environmental science [31,32] and biomedical chemistry [33,34]. In recent years, the wider application of CNTs is anticipated and continues to increase according to the reported data [35]. To optimize the use of CNTs in various applications, the attachment of functional groups or other nanostructures onto their surface is always important and necessary [36]. The combination of CNTs with various inorganic nonmetal/metal oxide nanoparticles including SiO_2 [37], SnO_2 [38,39], Fe_3O_4 [40], Al_2O_3 [41], TiO_2 [42] and so on through interfacial engineering has opened up some new possibilities for designing novel nanocomposites with superior performances, and the degradation degrees were highly enhanced over that of the controls, as-prepared metal oxide nanoparticles. The introduction of CNTs into TiO_2 could help to improve its photodegradation efficiency [43].

In addition, the crystalline phase composition, Schottky barrier structure, microstructure and electrical properties of TiO_2-based composites could also be affected by doping with rare earth [44] and other metal oxides [45,46]. The photodegradation of the organic dyes into nontoxic small molecules is anticipated [11,47–51].

To improve their photodegradation efficiencies, herein, we hope to develop novel TiO_2-based composites by simultaneous introduction of both CNTs and Eu^{3+}. The chemical composition, morphology and crystalline phase of the composites were measured by several testing methods. The photodegradation properties of the composites toward three kinds of organic dyes including MB, MO and RhB were investigated. The possible photodegradation mechanism was also proposed.

2. Methods and materials

2.1. Chemicals and materials

Tetrabutyl titanate ($C_{16}H_{36}O_4Ti$; TBOT; AR) and acetic acid (CH_3COOH; AR) were obtained from Sinopharm Group Co., Ltd., China. Multi-walled CNTs (MWCNTs) with mean diameters of 20–40 nm, specific surface areas of 90–120 m^2/g and purity higher than 97.0% were provided by Shenzhen Nanotech Port Co., Ltd., China. Europium trichloride ($EuCl_3$; 99.99%) was purchased from Shandong Xiya Chemicals Co., Ltd., China. MB, RhB and MO were purchased from Chengdu Xiya Chemical Technology Co., Ltd., China. Other reagents were all of analytical grade and used without further purification. Deionized water used in all experiments was obtained from the Milli-Q water purification system.

2.2. Preparation of TiO_2 nanoparticles

The TiO_2 nanoparticles were prepared by a sol–gel method as follows: (1) Under magnetic stirring, 15 mL of TBOT was added to a mixture of ethanol (45 mL) and acetic acid (3 mL). The reaction was kept for 30 min to obtain a transparent solution A. (2) In a 100 mL beaker, 30 mL of ethanol was added, then 15 mL of deionized water and 1 mL of concentric nitric acid was added to the solution in order, and the mixture was stirred to obtain another transparent solution B. (3) Under vigorous stirring, the solution A was slowly added into the solution B, and the obtained mixture was heated to 80°C for 1 h. After that, the prepared TiO_2 nanometer sol was washed using deionized water and ethanol for at least three times. The residual white solid on the filter paper was dried in a vacuum oven at 100°C for 4 h to obtain the TiO_2 precursor. (4) The TiO_2 precursor was added in a muffle furnace, which was heated to 450°C at a heating rate of about 5°C/min. And the TiO_2 nanoparticles were obtained by calcination of the TiO_2 precursor at 450°C for 2 h.

2.3. Preparation of TiO_2-based nanocomposites

2.3.1. Purification of MWCNTs

The oxidized MWCNTs (ox-MWCNTs) were prepared according to the reported methods [52]. In brief, 300 mg of MWCNTs were mixed with 100 mL of concentrate nitric acid, which was heated to 120°C and reacted for 24 h. After that, the reaction was cooled to ambient temperature. The mixture was filtered, and subsequently washed repeatedly using deionized water, ethanol and ethyl ether. The black solid residual on the filter paper was dried at 100°C for 48 h to obtain 286 mg of ox-MWCNTs.

2.3.2. Preparation of ox-MWCNT/TiO_2 composites

The ox-MWCNT/TiO_2 composites were prepared according to the same method as previously mentioned (see, section 2.2), only the solution B contains another constituent, 0.1515 g of ox-MWCNTs. And the ox-MWCNT/TiO_2 composites were obtained by calcination of the ox-MWCNT/TiO_2 precursor at 450°C for 2 h.

2.3.3. Preparation of Eu^{3+}/ox-MWCNT/TiO_2 composites

The ox-MWCNT/TiO_2 and Eu^{3+}/ox-MWCNT/TiO_2 composites were prepared according to the same method as previously mentioned (see, section 2.3.2), and the solution B also contains another constituent, $EuCl_3$ (the mass percentage of Eu^{3+} is 1% and 4%, respectively). And the Eu^{3+}/ox-MWCNT/TiO_2 composites were obtained by calcination of the precursor

at 450°C for 2 h, and the obtained composites were assigned as 1% Eu^{3+}/ox-MWCNT/TiO_2 and 4% Eu^{3+}/ox-MWCNT/TiO_2, respectively.

2.4. Measurements and characterizations

2.4.1. Microscopic observation

The morphologies of ox-MWCNT/TiO_2 composites, Eu^{3+}/ox-MWCNT/TiO_2 composites and TiO_2 nanoparticles were examined by high-resolution transmission electron microscopy (HR-TEM) on a JEM-2100F instrument (JEOL, Japan) under an acceleration voltage of 200 kV, and the samples were prepared by fine dispersion of ethanolic suspensions of TiO_2-based photocatalyst onto holey amorphous carbon films of the Cu TEM grids and then vaporizing ethanol.

2.4.2. Spectral analysis

The structural changes of TiO_2 after impregnation of Eu^{3+} and ox-MWCNTs were measured by X-ray diffractometer (XRD) with Cu *Kα* radiation (λ = 0.154056 nm) under a voltage of 40 kV and a current of 250 mA on a *D*/Max-RA X-ray diffractometer (Rigaku, Japan). Energy-dispersive X-ray (EDX) spectroscopy was measured using a 200 kV JEM-2100F microscope (JEOL, Japan) operating at 200 kV.

2.4.3. Photocatalytic degradation tests

The photocatalytic degradation of three organic dyes including MB, RhB and MO by the TiO_2 nanoparticles, ox-MWCNT/TiO_2 composite and the two Eu^{3+}/ox-MWCNT/TiO_2 composites was measured on a BL-GHX-I photochemical reactions instrument (Shanghai Bilon Precision Instruments Co., Ltd., China). All the photocatalytic degradation results presented in this work are the mean of three replicates.

MB, RhB and MO aqueous solutions (10 mg/L) were prepared and stored in the refrigerator for future use. Batch degradation experiments were performed in Pyrex glass screw-cap tubes. 500 mg of TiO_2, ox-MWCNTs/TiO_2 or Eu^{3+}/ox-MWCNT/TiO_2 was placed into the reactors containing 250 mL of dye solutions, respectively. The reactions were stirred and irradiated by the light with the wavelength of 365 nm which was emitted from a high pressure mercury lamp (125 W). The concentrations of dyes were analyzed using a UV-visible absorption spectrometer using the light of 664, 554 and 464 nm for MB, RhB and MO, respectively.

Illuminated with the light from a high pressure mercury (Hg) lamp (λ = 365 nm), the photodegradation of MB, MO and RhB was carried for 10, 30, 60, 90 and 120 min. The photodegradation of organic dyes by using as-prepared TiO_2, ox-MWCNT/TiO_2, 1% Eu^{3+}/ox-MWCNT/TiO_2 and 4% Eu^{3+}/ox-MWCNT/TiO_2 was investigated. The degradation efficiency (*R*) could be calculated using the following Eq. (1):

$$R(\%) = \frac{C_0 - C}{C_0} \times 100 \quad (1)$$

where C_0 is the initial concentration of the dye solution (mg/L), *C* is the concentration of the dye solution at different time intervals after photodegradation (mg/L).

2.4.4. Contrast adsorption experiments

The dark adsorption of dyes on the surface of the catalysts might affect the final evaluation of the photocatalytic activity of these materials. The amount of adsorbed dyes should be determined when the adsorption equilibrium was reached before the photocatalytic experiments were performed. By placing the tubes which contain dye solutions and the TiO_2-based catalysts in dark, parallel tests were used to evaluate the adsorption capabilities of the catalysts.

3. Results and discussion

3.1. Characterization results

3.1.1. X-ray diffraction

As shown in Fig. 2, XRD patterns of TiO_2, ox-MWCNT/TiO_2, 1% Eu^{3+}/ox-MWCNT/TiO_2 and 4% Eu^{3+}/ox-MWCNT/TiO_2 all exhibited six characteristic XRD peaks at 2θ = 25.3°, 37.8°, 48.0°, 53.9°, 55.0° and 62.6°. In contrast to the JPCDS card of NO21-1272 which shows XRD peaks at 2θ = 25.3°, 37.8°, 48.0°, 53.9°, 55.0° and 62.5°, which correspond to the crystal planes (101), (004), (200), (105), (211), (204), (220) and (215) of the anatase phase of TiO_2. Additionally, the characteristic XRD peak of MWCNTs is 25.9° (plane 002), which was superposed by the diffraction lines of anatase TiO_2 at 25.3° (plane 101). The average grain sizes of TiO_2, ox-MWCNT/TiO_2, 1% Eu^{3+}/ox-MWCNT/TiO_2 and 4% Eu^{3+}/ox-MWCNT/TiO_2 were calculated as 11.7, 15.9, 11.0 and 8.9 nm, respectively.

3.1.2. Transmission electron microscopy

TEM images could provide information on the morphology and crystallinity of the samples. As shown in Fig. 3, the particle sizes of the as-prepared TiO_2 (Figs. 3(A) and (B)), 1% Eu^{3+}/ox-MWCNT/TiO_2 (Figs. 3(C) and (D)) and 4% Eu^{3+}/ox-MWCNT/TiO_2 (Fig. 3(E)) are homogeneous with the diameter of 10–15 nm. Obviously, TiO_2 nanoparticles are well distributed on the surface of ox-MWCNTs (Figs. 3(C) and (E)).

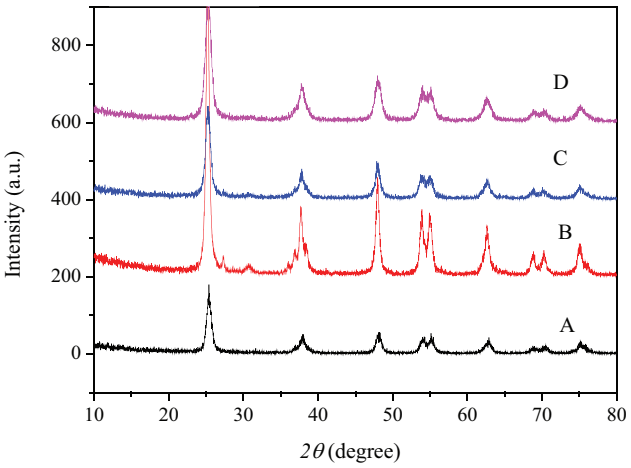

Fig. 2. XRD pattern of the samples: (A) TiO_2; (B) ox-MWCNT/TiO_2; (C) 1% Eu^{3+}/ox-MWCNT/TiO_2 and (D) 4% Eu^{3+}/ox-MWCNT/TiO_2.

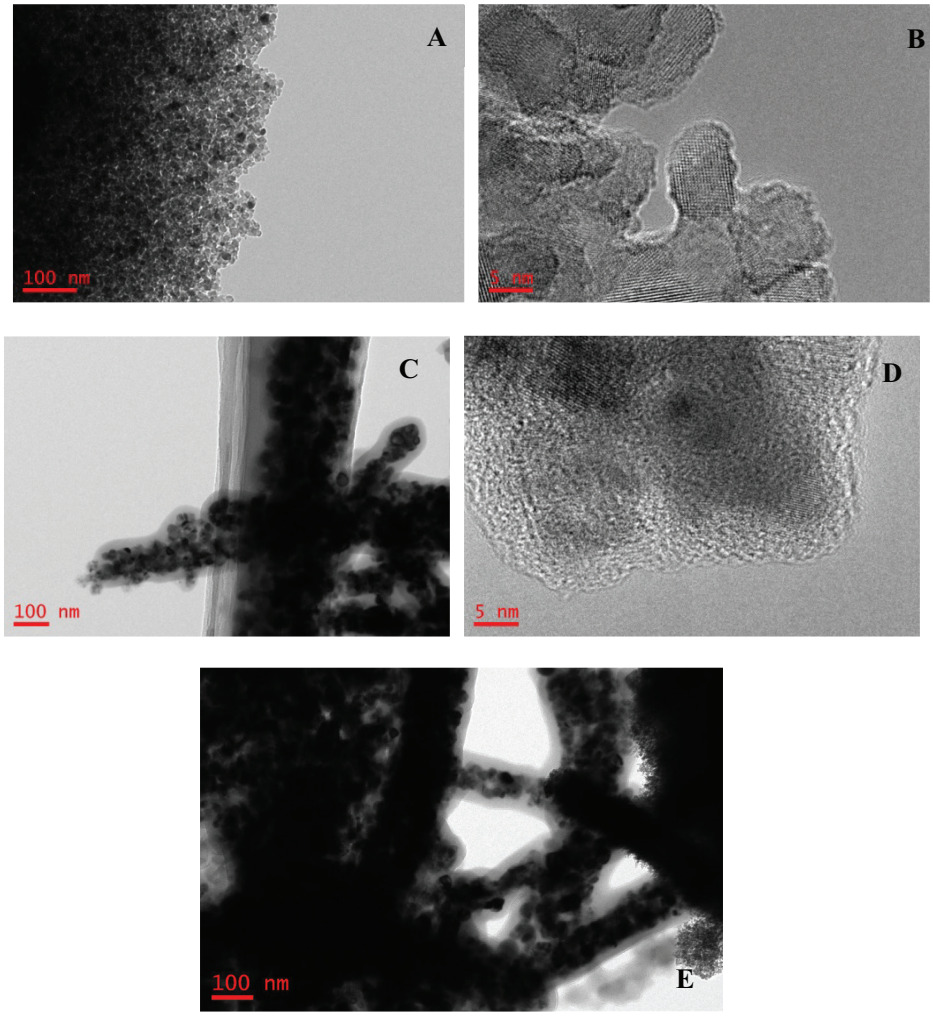

Fig. 3. TEM images of the samples: (A) TiO_2 (low-resolution); (B) TiO_2 (high-resolution); (C) 1% Eu^{3+}/ox-MWCNT/TiO_2 (low-resolution); (D) 1% Eu^{3+}/ox-MWCNT/TiO_2 (high-resolution) and (E) 4% Eu^{3+}/ox-MWCNT/TiO_2.

3.1.3. EDX spectroscopy analysis

EDX spectroscopy could provide information on the chemical composition of the samples. As shown in Fig. 4(A), around 63.40 At% of O and 36.60 At% of Ti are found in as-prepared TiO_2, indicating that the atomic ratio of O to Ti is close to 2.

As shown in Fig. 4(B), about 0.98 wt% of Eu and 18.90 wt% of carbon (C) are involved in 1% Eu^{3+}/ox-MWCNT/TiO_2 composite. For the 4% Eu^{3+}/ox-MWCNT/TiO_2 composite, about 3.65 wt% of Eu and 19.70 wt% of carbon were detected (Fig. 4(C)). The EDX spectroscopy analysis confirmed the introduced Eu and C.

3.2. Photodegradation of three kinds of dyes

3.2.1. Photodegradation of MB

As shown in Fig. 5, the photodegradation of MB was better catalyzed by the 1% Eu^{3+}/ox-MWCNT/TiO_2, followed by ox-MWCNT/TiO_2, then by 4% Eu^{3+}/ox-MWCNT/TiO_2, and finally by the as-prepared TiO_2. According to the results, we can infer that adding MWCNTs is helpful and effective for improving the photochemical activity of TiO_2-based composite. Meanwhile, the dosage of Eu doping would also affect the photochemical activity of TiO_2-based composite, and the ox-MWCNTs/TiO_2 composites with appropriate dosage of Eu doping possessed better photochemical activity. However, too much Eu doping would decrease the composite's photochemical activity.

3.2.2. Photodegradation of MO

The photodegradation of MO was carried out under irradiation at 365 nm for 2 h. As shown in Fig. 6, the 1% Eu^{3+}/ox-MWCNT/TiO_2 composite has the best degradation effect, and similarly the dose of Eu could affect its photochemical activity.

3.2.3. Photodegradation of RhB

The photochemical activities of TiO_2, 4% Eu^{3+}/ox-MWCNT/TiO_2, ox-MWCNTs/TiO_2 and 1% Eu^{3+}/ox-MWCNT/TiO_2 toward RhB were also evaluated. As shown in Fig. 7,

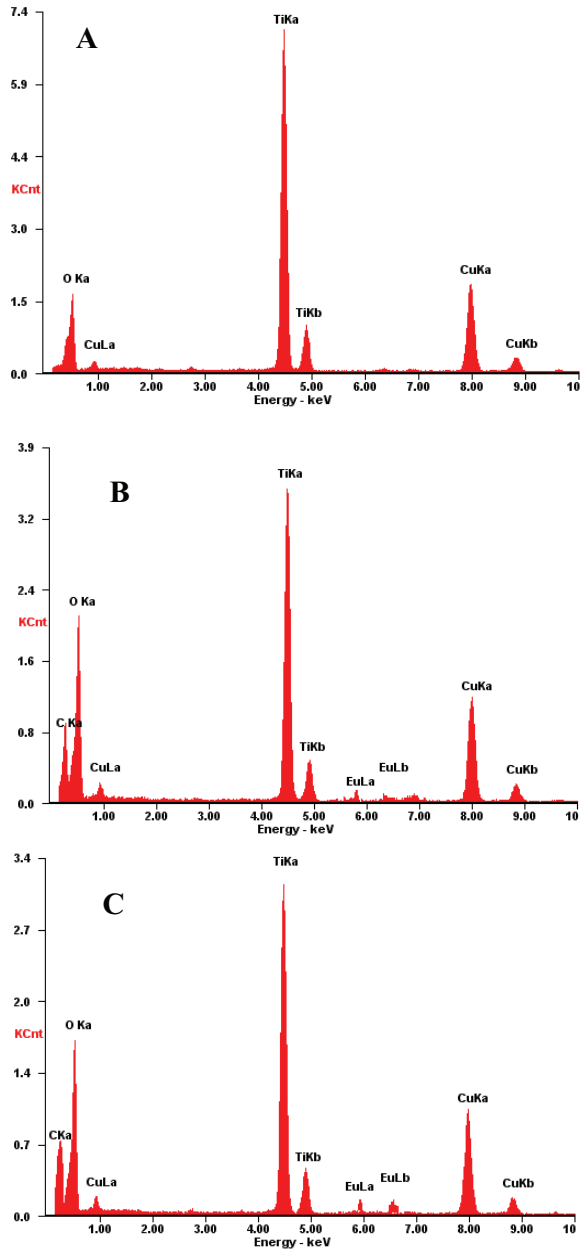

Fig. 4. EDX of the samples: (A) TiO_2; (B) 1% Eu^{3+}/ox-MWCNT/TiO_2 and (C) 4% Eu^{3+}/ox-MWCNT/TiO_2.

ox-MWCNT/TiO_2 showed the highest degradation percentage. However, 4% Eu^{3+}/ox-MWCNTs/TiO_2 and 1% Eu^{3+}/ox-MWCNTs/TiO_2 also exhibited similar degradation capabilities which were higher than that of pristine TiO_2, indicating the introduction of ox-MWCNTs and Eu doping were very beneficial to improving the catalysts' photocatalysis ability.

3.2.4. Comparisons of capabilities of the catalysts

The photochemical activities of TiO_2, 4% Eu^{3+}/ox-MWCNT/TiO_2, MWCNTs/TiO_2 and 1% Eu^{3+}/ox-MWCNTs/TiO_2 toward MB, RhB and MO were compared. As shown in Figs. 5–7, MB could be better degraded

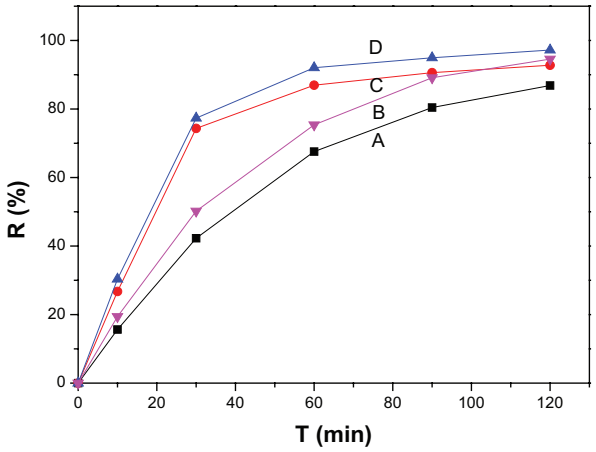

Fig. 5. Photodegradation of MB using TiO_2-based catalysts: (A) TiO_2; (B) ox-MWCNT/TiO_2; (C) 4% Eu^{3+}/ox-MWCNT/TiO_2 and (D) 1% Eu^{3+}/ox-MWCNT/TiO_2.

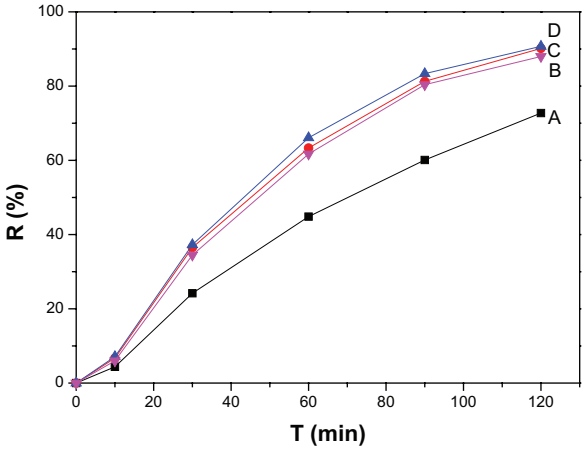

Fig. 6. Photodegradation of MO using TiO_2-based catalysts: (A) TiO_2; (B) 4% Eu^{3+}/ox-MWCNT/TiO_2; (C) ox-MWCNTs-TiO_2 and (D) 1% Eu^{3+}/ox-MWCNT/TiO_2.

than RhB and MO by TiO_2. Similarly, the results obtained by using 4% Eu^{3+}/ox-MWCNT/TiO_2, ox-MWCNT/TiO_2 and 1% Eu^{3+}/ox-MWCNT/TiO_2 as the catalysts were nearly identical to that of obtained by using pristine TiO_2, indicating that MB was easier to be photodegraded by the catalysts. Usually, the structure of a dye decides its nature of photodegradation properties. As shown in Fig. 1, both RhB and MB are cationic dyes, and the interactions among the highly delocalized conjugated system of MWCNTs and the dyes facilitate their adsorption, resulting in the enhanced photodegradation efficiencies. In addition, the phenothiazine framework of MB is a photoactive center, which is potentially more vulnerable to degradation than that of MO and RhB [53].

3.3. Verification of the photodegradation

To verify that the decreased organic dye concentrations mainly originated from the photodegradation rather than adsorption, the contact of MB in the dark using TiO_2 and 1%

Eu^{3+}/ox-MWCNT/TiO_2 were investigated. As shown in Fig. 8, the adsorption could reach the equilibrium in about 60 min, the adsorption rates of MB by TiO_2 and 1% Eu^{3+}/ox-MWCNT/TiO_2 are 4% and 16%, respectively, indicating that the adsorption capacities of the TiO_2-based adsorbents are relatively very low.

3.4. Contrast experiments

In order to verify the catalytic activity of the photocatalytic materials, the photodegradation of MB was carried out without adding any catalysts. As shown in Fig. 9, the photodegradation efficiency decreases obviously. Only 12 wt% of MB was degraded after irradiation for 5 h, indicating that the catalytic activities of the TiO_2 based are superior.

3.5. Photodegradation kinetics

To better describe the photocatalytic degradation process, the data were fitted by a dynamic mode, Langmuir–Hinshelwood (LH) kinetics [54]. It is well-known that LH kinetics is one of the most commonly used kinetic expressions to explain the kinetics of a heterogeneous catalytic process. LH kinetics describes that the rate of a heterogeneous reaction is mainly controlled by the reaction of the adsorbed molecules, and that all adsorption and desorption pressure are in equilibrium:

$$r = -\frac{dc}{dt} = \frac{K_r KC}{1 + KC} \tag{2}$$

or

$$\frac{1}{r} = \frac{1}{K_r} + \frac{1}{K_r KC} \tag{3}$$

where r is rate of reaction [mg/(L·min)]; C is the concentration at any time t during degradation (mg/L); K_r is limiting rate constant of reaction at maximum coverage under the given experimental conditions (h^{-1}); K is the equilibrium constant for adsorption of the substrate onto catalyst and t is contact time (min).

And K could be calculated by the following equation:

$$\ln\left(\frac{C}{C_0}\right) + K(C - C_0) = -K_r Kt \tag{4}$$

where C_0 is the initial dye concentration (mg/L).

Due to the adsorption in dark and adsorption/desorption under illumination, the apparent rate constant (K') would be less than K_r:

$$r = -\frac{dc}{dt} = K_r KC = K'C \tag{5}$$

The pseudo-first-order kinetic model and the half-life of reactants ($t_{1/2}$) could be described as follows, respectively:

$$\ln\left(\frac{C}{C_0}\right) = -K_r Kt = -K't \tag{6}$$

$$t_{1/2} = \frac{\ln 2}{K'} \tag{7}$$

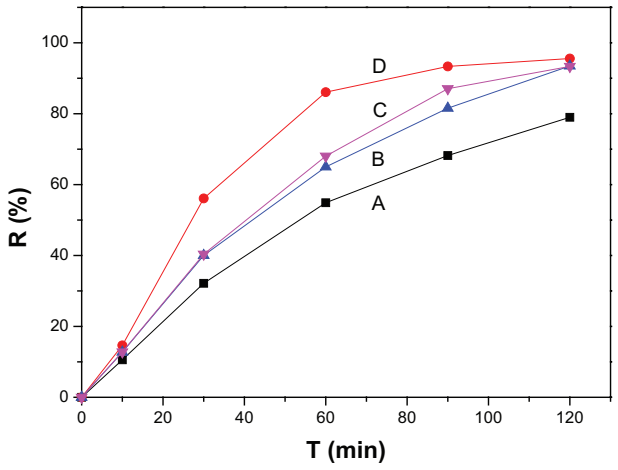

Fig. 7. Photodegradation of RhB using TiO_2-based catalysts: (A) TiO_2; (B) 4% Eu^{3+}/ox-MWCNT/TiO_2; (C) 1% Eu^{3+}/ox-MWCNT/TiO_2 and (D) ox-MWCNT/TiO_2.

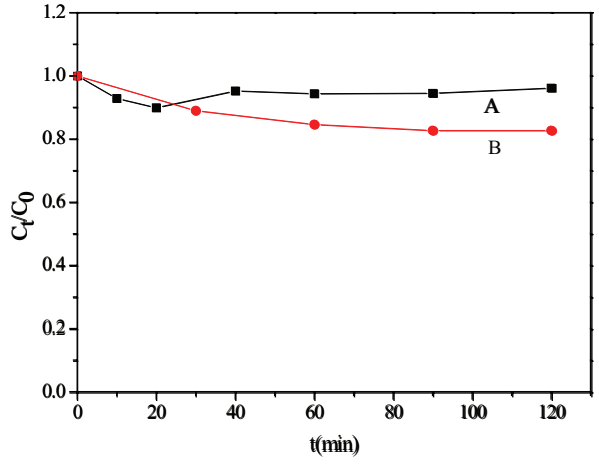

Fig. 8. Adsorption of MB in the dark: (A) TiO_2 and (B) 1% Eu^{3+}/ox-MWCNT/TiO_2.

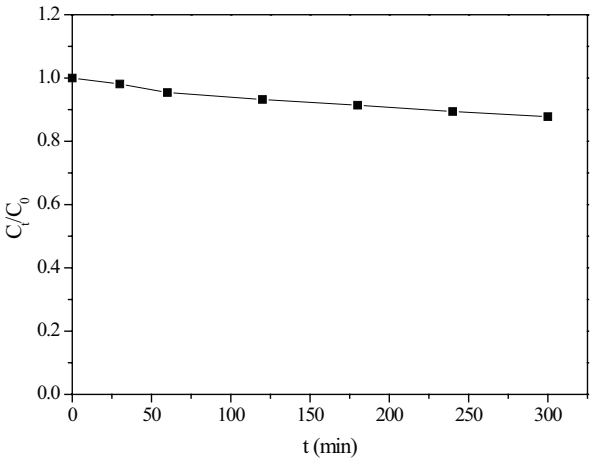

Fig. 9. Photodegradation of MB without adding any photocatalytic materials.

By fitting the kinetic curves at various contact time, the K' of various catalysts could be obtained in plots of $\ln(C/C_0)$ vs. t (Fig. 10 and Table 1).

As shown in Fig. 10, the data of the photocatalytic degradation of MB by TiO_2, ox-MWCNT/TiO_2, 1% Eu^{3+}/ox-MWCNT/TiO_2 and 4% Eu^{3+}/ox-MWCNT/TiO_2 are all fitted well by the pseudo-first-order kinetics model. The correlation of determination (R^2) is all close to 1, indicating the linear relationships are good. From Table 1, it could be found that the reaction rate constant, K', increases in the following order of TiO_2 < 4% Eu^{3+}/ox-MWCNT/TiO_2 < ox-MWCNTs/TiO_2 < 1% Eu^{3+}/ox-MWCNT/TiO_2, indicating the introduction of Eu or MWCNTs contributed to the photocatalytic activity. However, too much of Eu doping would decrease the catalyst's activity. Simultaneously, the $t_{1/2}$ of 1% Eu^{3+}/ox-MWCNT/TiO_2 is the shortest, demonstrating once again the doping of appropriate amounts of MWCNTs and Eu can improve the catalytic effects of the catalysts.

3.6. Photodegradation mechanism

From the prior reported results, a possible mechanism for the photodegradation of organic dyes by TiO_2-based composite was also proposed.

Due to the adsorption capability for dyes and being suitable for promoting photo-induced electrons transfer, the load of TiO_2 on the ox-MWCNTs can highly improve its photocatalytic efficiency [43]. The doping of Eu^{3+} can also improve the catalysts' photocatalytic efficiencies because Eu^{3+} doping can form the lattice distortion for TiO_2, producing oxygen vacancy for the generation of free radicals. In addition, the 5d unoccupied orbital of Eu^{3+} could provide transfer place for the photo-induced electrons and restrain the electron-cavity compounding speed (Fig. 11). However, the excessive doping of Eu^{3+} would form more surface defects and produce more electron-cavity compounding centers, thereby reducing the photocatalytic efficiencies of the catalysts [55].

It could be speculated that a direct transition of electrons from valence band to the conduction band on the surface of the catalysts after absorbing the light rays would lead to the production of electron/hole pairs [56–58]. The electrons transfer to ox-MWCNTs and Eu^{3+}, producing free radicals of $\cdot O_2^-$ by reaction with the adsorbed O_2. The photogenerated holes would react with OH^- to produce free radicals of ·OH. These generated free radicals would react with the organic dyes to realize the highly efficient photodegradation (Eqs. (8)–(11)).

$$\mathrm{Eu/TiO_2-MWCNTs + hv \rightarrow Eu/TiO_2-MWCNTs}(e_{CB}^- + h_{VB}^+) \quad (8)$$

$$\mathrm{Eu/TiO_2-MWCNTs}(e_{CB}^-) + O_2 \rightarrow \mathrm{Eu/TiO_2-MWCNTs} + \cdot O_2^- \quad (9)$$

$$\mathrm{Eu/TiO_2-MWCNTs}(h_{VB}^+) + OH^- \rightarrow \mathrm{Eu/TiO_2-MWCNTs} + \cdot OH \quad (10)$$

$$\cdot OH(\cdot O_2^-) + \mathrm{dyes} \rightarrow \mathrm{degradation\ product} \quad (11)$$

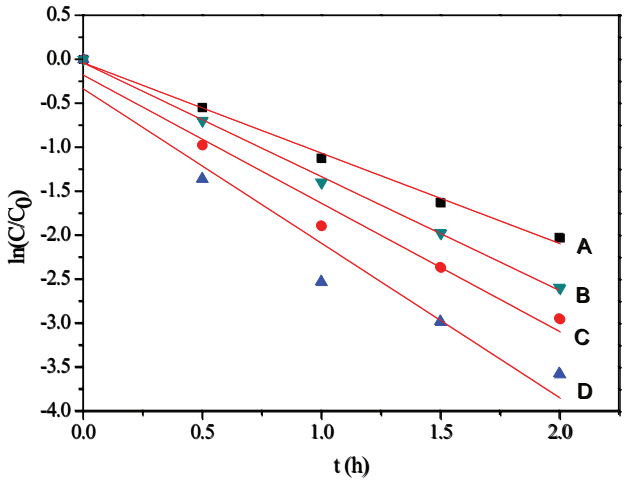

Fig. 10. The fitting kinetic curves of different catalysts toward MB: (A) TiO_2; (B) 4% Eu^{3+}/ox-MWCNT/TiO_2; (C) ox-MWCNT/TiO_2 and (D) 1% Eu^{3+}/ox-MWCNT/TiO_2.

4. Conclusions

The preparation of several TiO_2-based composites for photodegradation of three kinds of organic dyes including MO, MB and RhB was carried out. The TiO_2-based composites were fully characterized using XRD, TEM and EDX. The doping of ox-MWCNTs and ox-MWCNT/Eu^{3+} could improve their photodegradation performance. And the 1% Eu^{3+}/ox-MWCNT/TiO_2 composite showed higher photodegradation rate constant (K' = 1.757 h^{-1}) than those of pristine TiO_2 (K' = 1.028 h^{-1}), ox-MWCNT/TiO_2 (K' = 1.458 h^{-1}) and 4% Eu^{3+}/ox-MWCNT/TiO_2 composite (K' = 1.295 h^{-1}) toward MB. Simultaneous, the 1% Eu^{3+}/ox-MWCNT/TiO_2 composite possessed high photodegradation percentage of 95.77%, 97.21% and 90.72% toward RhB, MB and MO, respectively, which were higher than those of other three TiO_2-based photocatalysts. The photodegradation mechanism was also proposed. The developed TiO_2-based composites have showed potential application prospects in treating organic dyes contaminated wastewater in the future.

Table 1
The fitting rate equations of different catalysts' photocatalytic kinetics

Photocatalysts	Fitting rate equation	K' (h^{-1})	R^2	$t_{1/2}$(h)
TiO_2	$y = -1.028x - 0.039$	1.028	0.994	0.674
ox-MWCNTs/TiO_2	$y = -1.458x - 0.179$	1.458	0.970	0.475
1% Eu^{3+}/ox-MWCNT/TiO_2	$y = -1.757x - 0.335$	1.757	0.934	0.394
4% Eu^{3+}/ox-MWCNT/TiO_2	$y = -1.295x - 0.040$	1.295	0.998	0.535

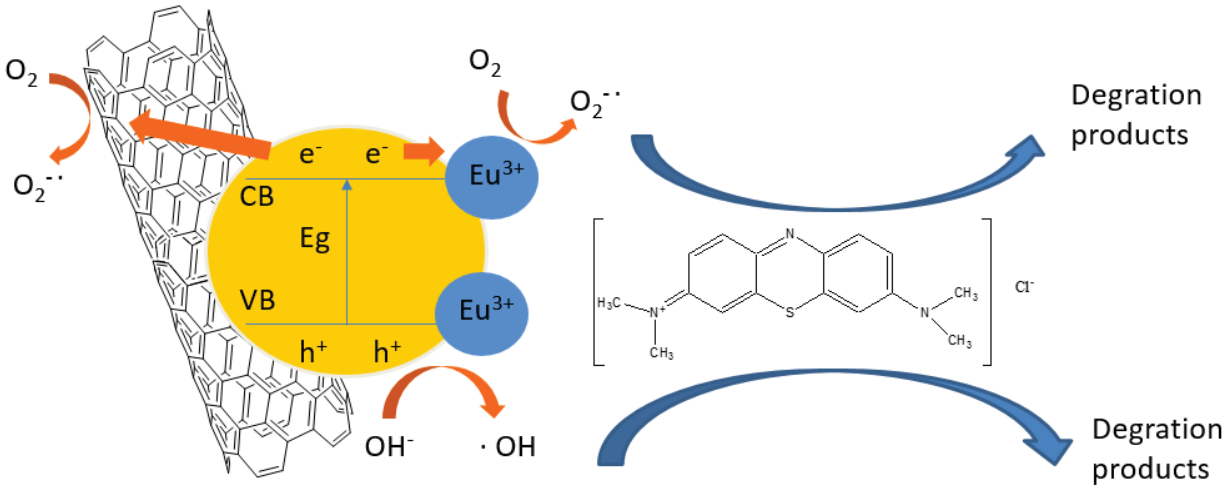

Fig. 11. The proposed degradation mechanism.

Acknowledgments

Financial supports from National Natural Science Foundation of China (Nos. 21471163, 51674292 and 21571191), Provincial Natural Science Foundation of Hunan (No. 2016JJ1023), Project of Innovation-driven Plan in Central South University (No. 2016CX007) and Hunan Provincial Science and Technology Plan Project, China (No. 2016TP1007) are greatly appreciated.

References

[1] T. Nasrabadi, An index approach to metallic pollution in river waters, Int. J. Environ. Res., 9 (2015) 385–394.
[2] O.S. Bello, K.A. Adegoke, A.A. Olaniyan, H. Abdulazeez, Dye adsorption using biomass wastes and natural adsorbents: overview and future prospects, Desal. Wat. Treat., 53 (2015) 1292–1315.
[3] N. Guo, Y.M. Liang, S. Lan, L. Liu, G.J. Ji, S.C. Gan, H.F. Zou, X.C. Xu, Uniform TiO_2–SiO_2 hollow nanospheres: synthesis, characterization and enhanced adsorption–photodegradation of azo dyes and phenol, Appl. Surf. Sci., 305 (2014) 562–574.
[4] W. Konicki, K. Cendrowski, X.C. Chen, E. Mijowska, Application of hollow mesoporous carbon nanospheres as an high effective adsorbent for the fast removal of acid dyes from aqueous solutions, Chem. Eng. J., 228 (2013) 824–833.
[5] J.H. Deng, X.R. Zhang, G.M. Zeng, J.L. Gong, Q.Y. Niu, J. Liang, Simultaneous removal of Cd(II) and ionic dyes from aqueous solution using magnetic graphene oxide nanocomposite as an adsorbent, Chem. Eng. J., 226 (2013) 189–200.
[6] U.G. Akpan, B.H. Hameed, Parameters affecting the photocatalytic degradation of dyes using TiO_2-based photocatalysts: a review, J. Hazard. Mater., 170 (2009) 520–529.
[7] A. Buthiyappan, A. Aziz, A. Raman, W. Daud, W.M. Ashri, Recent advances and prospects of catalytic advanced oxidation process in treating textile effluents, Rev. Chem. Eng., 32 (2016) 1–47.
[8] M.N. Chong, B. Jin, C.W.K. Chow, C. Saint, Recent developments in photocatalytic water treatment technology: a review, Water Res., 44 (2010) 2997–3027.
[9] Z. Zhang, F. Xiao, J. Xiao, S. Wang, Functionalized carbonaceous fibers for high performance flexible all-solid-state asymmetric supercapacitors, J. Mater. Chem. A, 3 (2015) 11817–11823.
[10] S. Yu, X. Wang, Z. Chen, J. Wang, S. Wang, T. Hayat, X. Wang, Layered double hydroxide intercalated with aromatic acid anions for the efficient capture of aniline from aqueous solution, J. Hazard. Mater., 321 (2017) 111–120.
[11] M. Karimi-Shamsabadi, A. Nezamzadeh-Ejhieh, Comparative study on the increased photoactivity of coupled and supported manganese-silver oxides onto a natural zeolite nano-particles, J. Mol. Catal. A: Chem., 418 (2016) 103–114.
[12] S. Mousavi-Mortazavi, A. Nezamzadeh-Ejhieh, Supported iron oxide onto an Iranian clinoptilolite as a heterogeneous catalyst for photodegradation of furfural in a wastewater sample, Desal. Wat. Treat., 57 (2016) 10802–10814.
[13] Z.-A. Mirian, A. Nezamzadeh-Ejhieh, Removal of phenol content of an industrial wastewater via a heterogeneous photodegradation process using supported FeO onto nanoparticles of Iranian clinoptilolite, Desal. Wat. Treat., 57 (2016) 16483–16494.
[14] J. Esmaili-Hafshejani, A. Nezamzadeh-Ejhieh, Increased photocatalytic activity of Zn(II)/Cu(II) oxides and sulfides by coupling and supporting them onto clinoptilolite nanoparticles in the degradation of benzophenone aqueous solution, J. Hazard. Mater., 316 (2016) 194–203.
[15] A. Nezamzadeh-Ejhieh, Z. Banan, Photodegradation of dimethyldisulfide by heterogeneous catalysis using nanoCdS and nanoCdO embedded on the zeolite A synthesized from waste porcelain, Desal. Wat. Treat., 52 (2014) 3328–3337.
[16] F. Vasiliu, L. Diamandescu, D. Macovei, C.M. Teodorescu, D. Tarabasanu-Mihaila, A.M. Vlaicu, V. Parvulescu, Fe- and Eu-doped TiO_2 photocatalytical materials prepared by high energy ball milling, Top. Catal., 52 (2009) 544–556.
[17] J.W. Shi, J.T. Zheng, P. Wu, Preparation, characterization and photocatalytic activities of holmium-doped titanium dioxide nanoparticles, J. Hazard. Mater., 161 (2009) 416–422.
[18] S. Lopez-Ayala, M.E. Rincon, H. Pfeiffer, Influence of copper on the microstructure of sol–gel titanium oxide nanotubes array, J. Mater. Sci., 44 (2009) 4162–4168.
[19] C.Y. Kuo, Prevenient dye-degradation mechanisms using UV/TiO_2/carbon nanotubes process, J. Hazard. Mater., 163 (2009) 239–244.
[20] G.G. Bessegato, J.C. Cardoso, M.V.B. Zanoni, Enhanced photoelectrocatalytic degradation of an acid dye with boron-doped TiO_2 nanotube anodes, Catal. Today, 240 (2015) 100–106.
[21] R.C. Hsiao, N.S. Arul, D. Mangalaraj, R.S. Juang, Influence of Eu^{3+} doping on the degradation property of TiO_2 nanostructures, J. Optoelectron. Adv. Mater., 12 (2010) 193–198.
[22] Y.X. Li, T.H. Wang, S.Q. Peng, G.X. Lu, S.B. Li, Synergistic effect of Eu^{3+} and Si^{4+} co-doping on photocatalytic activity of titanium dioxide, Acta Phys. Chim. Sin., 20 (2004) 1434–1439.
[23] M.A. Salam, R.M. Mohamed, A.Y. Obaid, Enhancement of titanium dioxide-manganese oxide nanoparticles photocatalytic activity by doping with multi-walled carbon nanotubes, Fullerenes Nanotubes Carbon Nanostruct., 22 (2014) 765–779.

[24] A. Nezamzadeh-Ejhieh, M. Bahrami, Investigation of the photocatalytic activity of supported ZnO–TiO_2 on clinoptilolite nano-particles towards photodegradation of wastewater-contained phenol, Desal. Wat. Treat., 55 (2015) 1096–1104.
[25] H. Zabihi-Mobarakeh, A. Nezamzadeh-Ejhieh, Application of supported TiO_2 onto Iranian clinoptilolite nanoparticles in the photodegradation of mixture of aniline and 2,4-dinitroaniline aqueous solution, J. Ind. Eng. Chem., 26 (2015) 315–321.
[26] A. Besharati-Seidani, Photocatalytic oxidation of an organophosphorus simulant of chemical warfare agent by modified TiO_2 nanophotocatalysts, Iran. J. Catal., 6 (2016) 447–454.
[27] A.W. Hauser, N. Mardirossian, J.A. Panetier, M. Head-Gordon, A.T. Bell, P. Schwerdtfeger, Functionalized graphene as a gatekeeper for chiral molecules: an alternative concept for chiral separation, Angew. Chem. Int. Ed., 53 (2014) 9957–9960.
[28] C. Chen, N. Hayazawa, S. Kawata, A 1.7 nm resolution chemical analysis of carbon nanotubes by tip-enhanced Raman imaging in the ambient, Nat. Commun., 5 (2014) 3312.
[29] Z.H. Wang, J.Y. Yang, X.W. Wu, X.Q. Chen, J.G. Yu, Y.P. Wu, Enhanced electrochemical performance of porous activated carbon by forming composite with graphene as high-performance supercapacitor electrode material, J. Nanopart. Res., 19 (2017) 77.
[30] Z.A. Wang, X.M. Zhang, X.W. Wu, J.G. Yu, X.Y. Jiang, Z.L. Wu, X. Hao, Soluble starch functionalized graphene oxide as an efficient adsorbent for aqueous removal of Cd(II): the adsorption thermodynamic, kinetics and isotherms, J. Sol-Gel Sci. Technol., 82 (2017) 440–449.
[31] J.G. Yu, X.H. Zhao, H. Yang, X.H. Chen, Q. Yang, L.Y. Yu, J.H. Jiang, X.Q. Chen, Aqueous adsorption and removal of organic contaminants by carbon nanotubes, Sci. Total Environ., 482 (2014) 241–251.
[32] J.G. Yu, L.Y. Yu, H. Yang, Q. Liu, X.H. Chen, X.Y. Jiang, X.Q. Chen, F.P. Jiao, Graphene nanosheets as novel adsorbents in adsorption, preconcentration and removal of gases, organic compounds and metal ions, Sci. Total Environ., 502 (2015) 70–79.
[33] H. Bao, Y. Pan, Y. Ping, N.G. Sahoo, T. Wu, L. Li, J. Li, L.H. Gan, Chitosan-functionalized graphene oxide as a nanocarrier for drug and gene delivery, Small, 7 (2011) 1569–1578.
[34] A.C.A. Wan, J.Y. Ying, Nanomaterials for in situ cell delivery and tissue regeneration, Adv. Drug Delivery Rev., 62 (2010) 731–740.
[35] H.L. Xu, L. Huang, Z.Y. Zhang, B.Y. Chen, H. Zhong, L.M. Peng, Flicker noise and magnetic resolution of graphene hall sensors at low frequency, Appl. Phys. Lett., 103 (2013) 112405.
[36] J.G. Yu, N. Chen, F.P. Jiao, Q. Liu, X.Y. Jiang, J.H. Jiang, X.Q. Chen, Chemical attachment of hydrogen iodide to carbon nanotubes, Sci. Adv. Mater., 7 (2015) 1021–1027.
[37] J.D. Whittaker, E.D. Minot, D.M. Tanenbaum, P.L. McEuen, R.C. Davis, Measurement of the adhesion force between carbon nanotubes and a silicon dioxide substrate, Nano Lett., 6 (2006) 953–957.
[38] T. Umeyama, M. Fujita, N. Tezuka, N. Kadota, Y. Matano, K. Yoshida, S. Isoda, H. Imahori, Electrophoretic deposition of single-walled carbon nanotubes covalently modified with bulky porphyrins on nanostructured SnO_2 electrodes for photoelectrochemical devices, J. Phys. Chem. C, 111 (2007) 11484–11493.
[39] F. Du, X.Q. Zuo, Q. Yang, B. Yang, G. Li, Z.L. Ding, M.Z. Wu, Y.Q. Ma, S.W. Jin, K.R. Zhu, Facile assembly of TiO_2 nanospheres/SnO_2 quantum dots composites with excellent photocatalyst activity for the degradation of methyl orange, Ceram. Int., 42 (2016) 12778–12782.
[40] Z. Huang, J. Li, Q. Chen, H. Wang, A facile carboxylation of CNT/Fe_3O_4 composite nanofibers for biomedical applications, Mater. Chem. Phys., 114 (2009) 33–36.
[41] A.J. Hart, A.H. Slocum, L. Royer, Growth of conformal single-walled carbon nanotube films from Mo/Fe/Al_2O_3 deposited by electron beam evaporation, Carbon, 44 (2006) 348–359.
[42] D.J. Cooke, D. Eder, J.A. Elliott, Role of benzyl alcohol in controlling the growth of TiO_2 on carbon nanotubes, J. Phys. Chem. C, 114 (2010) 2462–2470.
[43] A. Nourbakhsh, S. Abbaspour, M. Masood, S.N. Mirsattari, A. Vahedi, K.J.D. Mackenzie, Photocatalytic properties of mesoporous TiO_2 nanocomposites modified with carbon nanotubes and copper, Ceram. Int., 42 (2016) 11901–11906.
[44] S. Yildirim, M. Yurddaskal, T. Dikici, I. Aritman, K. Ertekin, E. Celik, Structural and luminescence properties of undoped, Nd^{3+} and Er^{3+} doped TiO_2 nanoparticles synthesized by flame spray pyrolysis method, Ceram. Int., 42 (2016) 10579–10586.
[45] Z. Zhu, C.T. Kao, B.H. Tang, W.C. Chang, R.J. Wu, Efficient hydrogen production by photocatalytic water-splitting using Pt-doped TiO_2 hollow spheres under visible light, Ceram. Int., 42 (2016) 6749–6754.
[46] A. Cordero-Garcia, J.L. Guzman-Mar, L. Hinojosa-Reyes, E. Ruiz-Ruiz, A. Hernandez-Ramirez, Effect of carbon doping on WO_3/TiO_2 coupled oxide and its photocatalytic activity on diclofenac degradation, Ceram. Int., 42 (2016) 9796–9803.
[47] S. Shukla, S. Chaudhary, A. Umar, G.R. Chaudhary, S.K. Kansal, S.K. Mehta, Surfactant functionalized tungsten oxide nanoparticles with enhanced photocatalytic activity, Chem. Eng. J., 288 (2016) 423–431.
[48] A. Nezamzadeh-Ejhieh, M. Karimi-Shamsabadi, Comparison of photocatalytic efficiency of supported CuO onto micro and nano particles of zeolite X in photodecolorization of Methylene blue and Methyl orange aqueous mixture, Appl. Catal., A, 477 (2014) 83–92.
[49] A. Nezamzadeh-Ejhieh, S. Hushmandrad, Solar photodecolorization of methylene blue by CuO/X zeolite as a heterogeneous catalyst, Appl. Catal., A, 388 (2010) 149–159.
[50] A. Nezamzadeh-Ejhieh, H. Zabihi-Mobarakeh, Heterogeneous photodecolorization of mixture of methylene blue and bromophenol blue using CuO-nano-clinoptilolite, J. Ind. Eng. Chem., 20 (2014) 1421–1431.
[51] A. Nezamzadeh-Ejhieh, N. Moazzeni, Sunlight photodecolorization of a mixture of Methyl Orange and Bromocresol Green by CuS incorporated in a clinoptilolite zeolite as a heterogeneous catalyst, J. Ind. Eng. Chem., 19 (2013) 1433–1442.
[52] X.H. Zhao, F.P. Jiao, J.G. Yu, Y. Xi, X.Y. Jiang, X.Q. Chen, Removal of Cu(II) from aqueous solutions by tartaric acid modified multi-walled carbon nanotubes, Colloids Surf., A, 476 (2015) 35–41.
[53] A.A. Skripchenko, S.J. Wagner, Inactivation of WBCs in RBC suspensions by photoactive phenothiazine dyes: comparison of dimethylmethylene blue and MB, Transfusion, 40 (2000) 968–975.
[54] M. Hasnat, M. Uddin, A. Samed, S. Alam, S. Hossain, Adsorption and photocatalytic decolorization of a synthetic dye erythrosine on anatase TiO_2 and ZnO surfaces, J. Hazard. Mater., 147 (2007) 471–477.
[55] J.K. Yan, K.Y. Kang, J.H. Du, G.Y. Gan, J.H. Yi, Grain boundary segregation and secondary-phase transition of (La,Nb)-codoped TiO_2 ceramic, Ceram. Int., 42 (2016) 11584–11592.
[56] P. Mohammadyari, A. Nezamzadeh-Ejhieh, Supporting of mixed ZnS-NiS semiconductors onto clinoptilolite nano-particles to improve its activity in photodegradation of 2-nitrotoluene, RSC Adv., 5 (2015) 75300–75310.
[57] M. Babaahamdi-Milani, A. Nezamzadeh-Ejhieh, A comprehensive study on photocatalytic activity of supported Ni/Pb sulfide and oxide systems onto natural zeolite nanoparticles, J. Hazard. Mater., 318 (2016) 291–301.
[58] H. Derikvandi, A. Nezamzadeh-Ejhieh, Increased photocatalytic activity of NiO and ZnO in photodegradation of a model drug aqueous solution: effect of coupling, supporting, particles size and calcination temperature, J. Hazard. Mater., 321 (2017) 629–638.